Crystal chemistry and hydrogen bonding of rustumite $Ca_{10}(Si_2O_7)_2(SiO_4)(OH)_2Cl_2$ with variable OH, Cl, F

Revision 1

RUNNING TITLE: Crystal chemistry of rustumite

Frank Gfeller[1], Thomas Armbruster[1], Evgeny V. Galuskin[2], Irina O. Galuskina[2], Biljana Lazic[1],Valentina B. Savelyeva[3], Aleksandr E. Zadov[4], Piotr Dzierżanowski[5], and Viktor M. Gazeev[6]

[1] Mineralogical Crystallography, Institute of Geological Sciences, University of Bern, Freiestrasse 3, CH-3012 Bern, Switzerland
[2] Department of Geochemistry, Mineralogy and Petrography, Faculty of Earth Sciences, University of Silesia, Będzińska 60, 41-200 Sosnowiec, Poland
[3] Institute of the Earth's Crust SB RAS, Lermontov st. 128, 664033 Irkutsk, Russia
[4] Science Research Centre "NEOCHEM", Altuf'evskoye Highway 43, Moscow, Russia
[5] Institute of Geochemistry, Mineralogy and Petrology, Warsaw University, al. Żwirki i Wigury 93, 02-089 Warszawa, Poland
[6] Institute of Geology of Ore Deposits, Petrography, Mineralogy and Geochemistry (IGEM) RAS, Staromonetny 35, Moscow, Russia

Three samples of the skarn mineral rustumite $Ca_{10}(Si_2O_7)_2(SiO_4)(OH)_2Cl_2$, space group $C2/c$ $a \approx 7.6$, $b \approx 18.5$, $c \approx 15.5$ Å, $\beta \approx 104°$) with variable OH,Cl, F content were investigated by electron microprobe, single-crystal X-ray structure refinements, and Raman spectroscopy. "Rust1_LCl" is a low chlorine rustumite $Ca_{10}(Si_2O_7)_2(SiO_4)(OH_{1.88}F_{0.12})(Cl_{1.28},OH_{0.72})$ from skarns associated with the Rize batholith near Ikizedere, Turkey. "Rust2_F" is a F-bearing rustumite $Ca_{10}(Si_2O_7)_2(SiO_4)(OH_{1.13}F_{0.87})(Cl_{1.96}OH_{0.04})$ from xenoliths in ignimbrites of the Upper Chegem Caldera, Northern Caucasus, Russia. "Rust3_LCl_F" represents a low-Cl, F-bearing rustumite $Ca_{10}(Si_2O_7)_2[(SiO_4)_{0.87}(H_4O_4)_{0.13}](OH_{1.01}F_{0.99})(Cl_{1.00}\,OH_{1.00})$ from altered merwinite skarns of the Birkhin massif, Baikal Lake area, Eastern Siberia, Russia. Rustumite from Birkhin massif is characterized by a significant hydrogarnet-like or fluorine substitution at the apices of the orthosilicate group, leading to specific atomic displacements. The crystal structures including hydrogen positions have been refined from single-crystal X-ray data to R1 = 0.0205 (Rust1_LCl), R1= 0.0295 (Rust2_F) and R1= 0.0243 (Rust3_LCl_F). Depletion in Cl and replacement by OH is associated with smaller unit-cell dimensions. The substitution of OH by F leads to shorter hydrogen bonds HO-H···F instead of HO-H···OH. Raman spectra for all samples have been measured and confirm slight strengthening of the hydrogen bonds with uptake of F.

KEYWORDS: rustumite, crystal chemistry, skarn mineralogy, crystal structure, OH-, F-,Cl- substitution, Raman spectroscopy , hydrogen bonds.

Introduction

Rustumite (a = 7.62 Å b = 18.55 Å c = 15.51 Å β = 104.33°, V =2124 Å^3, space group $C2/c$) from contact-metamorphosed Jurassic limestone at Kilchoan, on the northwest coast of Scotland, was originally defined as a new mineral of assumed $Ca_3Si_2O_7(OH)_2$ composition (Agrell 1965). Two metamorphic stages are reported at Kilchoan. A first high-temperature decarbonatisation stage with a high CO_2:H_2O ratio and a second hydrothermal stage with low CO_2:H_2O. Rustumite occurs in a zone between spurrite dominant and kilchoanite dominant assemblages and may carry inclusions of spurrite, melilite, or its alteration products, merwinite, larnite, rankinite, and kilchoanite (Agrell 1965). The observed paragenesis provides evidence that rustumite formed during the second stage between 500°C and 700°C (Agrell 1965). Rustumite is named after Rustum Roy, well known for his contributions to science ranging from experimental mineralogy, interdisciplinary material research to science politics (Komarneni, 2011).

The revised end-member formula $Ca_{10}(Si_2O_7)_2(SiO_4)(OH)_2(Cl)_2$ of rustumite was derived from the crystal structure solved by Howie and Ilyukin (1977) and Nevskii et al. (1979). Increased electron density at a supposed OH position was interpreted to be caused by chlorine. The structure was solved in the monoclinic space group $C2/c$ with Z = 4 and refined to $R1$= 7.4%.

Taner et al. (1977) reported rustumite from skarns associated with the Rize-batholite near Ikizdere, Eastern Turkey. Based on the mineralogical skarn assemblages and fluid-inclusion micro-thermometry Hezarkhani (2006) proposed two stages of metamorphism. Similar to the skarn at Kilchoan (Agrell 1965) a high-temperature contact-metamorphic event is followed by hydrothermal alteration with an aqueous fluid at ca. 400°C. Rustumite formed during the latter and is associated with epidote, tremolite, trabzonite, hillebrandite, tilleyte, killalaite, chlorite and low temperature vesuvianite (Hezarkhani 2006). The Cl content of rustumite from these skarns is ca. 5.4 wt.% (Hezarkhani 2006) which corresponds to 1.4 Cl per formula unit (pfu). Stoichiometric rustumite with 2 Cl pfu requires 7.59 wt. % Cl.

A rustumite bearing skarn near the La Negra mine, Quertaro, Mexico is formed by a Tertiary diorite intrusion in a late-Jurassic limestone host-rock (Kanazawa et al. 1997). Rustumite and wadalite associated with andradite, hydrogarnet, magnetite and calcite grew zonally within spurrite rocks. The chlorine concentration of rustumite in these rocks is 5.76 – 6.24 wt. % but still below the stoichiometric limit. Rustumite has also been found in the gehlenite-spurrite-skarn at Kushiro, Hiroshima Prefecture, Japan (Takechi et al. 2000) but analytical data are missing.

In addition, granitoids of the Dara-e-Noor Massif at the Kala-e-Asad deposit in Kandaghar, Afghanistan, intruded into dolomites and assimilated them. The primary gehlenite – spurrite skarn was subsequently altered to rocks containing vesuvianite, garnet and wollastonite, which were cut by veinlets of tilleyite (replacing spurrite) and rustumite (Bogomolov 1970). It was the single-crystal X-ray diffraction pattern of rustumite described by Bogomolov (1970), indexed with an orthorhombic cell (probably erroneously – due to twinning), which inspired Dornberger-Schiff and Organova (1971) and Dornberger-Schiff and Fichtner (1972) to hypothesize rustumite to be a member of an OD-groupoid family. However, the subsequent structural studies by Howie and Ilyukin (1977) and Nevskii et al. (1979) did not support this interpretation.

An artificial analogue of rustumite was reported from burnt waste piles, deposited in the Chelyabinsk coal basin, Southern Ural region, Russia (Zateeva et al. 2006). However, the provided electron-microprobe data (their Table 3, analyses no. 4 (E-25)) suggest an anhydrous Cl-bearing material with Ca/Si = 1.72. The Ca/Si ratio should be 2 for rustumite. Their analysis is more consistent with the composition of the new mineral rusinovite $Ca_{10}(Si_2O_7)_3Cl_2$ (Galuskin et al. 2011). Furthermore, formation of rustumite under pyrometamorphic conditions is rather doubtful due to the low H_2O activity. Moreover, the occurrence of $Ca_{10}(Si_2O_7)_3Cl_2$ (analogue of rusinovite) from the dumps in the Chelyabinsk coal basin has been described before by Chesnokov et al. (1994). Chemical analyses of minerals in corroded refractory materials of waste combustion plants (Pawlowski 2008) were interpreted to show rustumite. Though confirmation by X-ray powder diffraction was not successful.

In summary, rustumite is a rare skarn mineral, which has not been reported from anthropogenic cementigeous materials. In this study, the variable chlorine-content of rustumite is investigated. The applied methods comprise single-crystal X-ray structure refinements, Raman spectroscopy, and electron microprobe analysis.

Sample description

Low-Cl rustumite (Rust1_LCl) was found in a hydrothermally altered skarn associated with the Rize-batholite near Ikizdere, Eastern Turkey. Detailed description of the geological context is provided by Taner et al., (1977), Sarp and Burri (1986), Sarp and Burri (1987), Hezarkhani (2006). The examined sample is part of the mineral collection of the Natural History Museum in Geneva, Switzerland (NHM Geneva accession number (477/051). Rustumite occurs

together with defernite, dellaite, spurrite, vesuvianite, hydrogrossular, foshagite and killalaite (Figure1a).

F-bearing rustumite (Rust2_F) with Cl content close to end-member occurs at the contact between xenolith no.1 (Galuskin et al. 2009) and unaltered ignibrites of the Upper Chegem Caldera, Northern Caucasus, Russia. Lens like rustumite-aggregates are surrounded by a bultfonteinite matrix (Figure 1b). In addition, at the contact to the ignimbrite wollastonite and rustumite form a thin transition zone. The rocks represent altered larnite exoskarns composed of cuspidine, hillebrandite, lakargiite, wadalite.

Rust3_LCl_F, a F-bearing, low-Cl rustumite forms symplectites together with monticellite replacing merwinite skarn of the Birkhin massif, Baikal Lake area, Eastern Siberia; Russia. A summary of the geological setting is reported by Lazic et al. (2011). Within the symplectite, clusters of clintonite and vesuvianite are observed (Figure 1c,d). In addition, larnite, merwinite, melilite, cuspidine, spurrite, bredigite, magnetite, perovskite, andradite and kerimasite occur in minor concentrations.

Experimental

Chemical analyses were carried out using an electron microprobe CAMECA SX100, (WDS mode, 15 kV, 10-20 nA, 1-3 μm beam diameter). Natural and synthetic standards were employed. The following lines and standards were used for rustumite analyses: Ca*K*α, Si*K*α – wollastonite; Fe*K*α – hematite, Ti*K*α – rutile, Mn*K*α – rhodochrosite; Mg*K*α – diopside; Na*K*α – albite, Al*K*α – orthoclase, S*K*α – barite, F*K*α – fluorphlogopite, Cl*K*α – tugtupite. For the sample Rust3_LCl_F from Birkhin the same crystals as used for structure refinement were analyzed with the electron-microprobe. For the other samples, analytical data were collected from crystals of the same thin section, from which also the structurally investigated crystals were extracted.

Raman spectra of all samples were recorded using a Dilor XY spectrometer equipped with a 1800 line mm^{-1} grating monochromator, a charge-coupled device (CCD), Peltier-cooled detector (1024×256) and an Olympus BX40 confocal microscope. The incident laser excitation was provided by a water-cooled argon laser source operating at 514.5 nm. The power at the exit of a 100x objective lens varied from 30 to 50 mW. Raman spectra were recorded in backscattering geometry in the range 100-4000 cm^{-1} with resolution of 2 cm^{-1}. Collection times of

20 s and accumulation of 5 scans were chosen. The monochromator was calibrated using the Raman scattering line of a silicon plate (520.7 cm^{-1}).

Single-crystal X-ray studies were carried out on three samples of rustumite low-Cl rustumite from Rize-batholite near Ikizdere (Rust1_LCl), F-bearing rustumite from the Chegem Caldera (Rust2_F), (Northern Caucasus) and low-Cl, F-bearing rustumite from Birkhin massif (Rust3_LCl_F), using a Bruker APEX II SMART diffractometer (MoKα, λ = 0.71073 Å). Experimental details are summarized in Table 1. Diffraction data were collected with ω scans at different φ settings (φ-ω scan) (Bruker, 1999). Data were processed using SAINT (Bruker, 1999). An empirical absorption correction using SADABS (Sheldrick, 1996) was applied. The structure was solved by direct methods with subsequent analyses of difference-Fourier maps. The rustumite structures were refined using the program SHELX97 (Sheldrick, 2008) to R1 = 2.05% (Rust1_LCl), R1 = 2.95% (Rust2_F) and 2.43 % (Rust3_LCl_F). The refinements including anisotropic atom displacement-parameters (except for H) have been carried out with neutral atom scattering-factors. If splitting of the Cl1 site was observed, two positions with common anisotropic displacement parameters were refined. The position with the longer distances to Ca was considered Cl and the one with the shorter distances was interpreted as O (OH). The occupancy of both sites were determined with the restraint OH + Cl = 1. Positions of the hydroxyl-group hydrogen atoms were derived from difference-Fourier syntheses. Subsequently, hydrogen positions were refined with restrained O-H distances of 0.96(2) Å. For Rust2_F no H-position has been refined, but a peak of 0.47 electrons near the predicted H2 site was observed in the difference Fourier-map. After standard refinement of the structure of rustumite from Birkhin (Rust3_LCl_F) we became aware of several inconsistencies compared to the previously refined rustumite samples: (1) residual density of about 2 electrons close to Ca2 suggested splitting of Ca2 into two subsites (Ca2 and Ca2A). (2) The mean <Si3-O> bond length within the orthosilicate group became 1.67 Å and was ca. 0.02 Å longer compared to the other samples. (3) The displacement parameter U_{eq} of Si3 was a factor of two larger than those of Si1 and Si2. In the other investigated samples displacement parameters of the three Si sites were similar to each other. (4) There was low residual density in difference-Fourier maps close to O4 and O8 (refined as subsites), which are the oxygen sites coordinating Si3. These findings (1-4) were interpreted with partial Si3 vacancies as known for a hydrogarnet-like substitution (Lager et al. 1987, Galuskin et al., 2007) or as a fluorine substitution at the subsites O4A and O8A . If the Si site is

empty the tetrahedron expands with 2 × O4A and 2 × O8A as tetrahedral apices. The splitting of original O4 into O4 and O4A also required splitting of Ca2 bonded to O4 and O4A. As a consequence of the hydrogarnet-type or F-substitution at the orthosilicate site, the occupancies of Si3, O4, O4A, O8, O8A, Ca2 and Ca2A were constrained to each other and refined with one variable. Subsequent refinements converged to Si3 occupancy of 0.876(4). We actually measured and refined structures of four rustumite crystals from Birkhin and all showed similar degree of hydrogarnet-like substitution.

The structure of rustumite possesses an alternative setting in space group *C*2/*c* with similar unit cell dimensions (a = 7.59, b = 18.58, c = 15.43 Å β = 103.82°). This second setting may be obtained from our setting (a = 7.59, b = 18.58, c = 15.49 Å β = 104.60°) by the transformation matrix (1 0 0, 0 -1 0, -1 0 -1). Due to the strong similarity in cell dimensions in both settings, pseudo-merohedral twinning according to the above matrix is common in rustumite. Corresponding twin refinements (1 0 0, 0 -1 0, -1 0 -1) converged to following fractions of twin individuals: 0.536(15) for Rust2_F and 0.005(5) for Rust3_LCl_F, respectively. The lower accuracy of cell dimensions for sample Rust2_F compared to the other studied rustumites is due to this pseudo-merohedral twinning.

Results

The electron-microprobe data is listed in Table 2. Variable Cl, F and OH contents are striking. The results for single-crystal structure refinement are summarised in Table 1, atomic coordinates and isotropic equivalents (U_{eq}) of anisotropic atom-displacement parameters in Tables 3 a-c, anisotropic atomic-displacement parameters in Tables 4 a-c (deposited material) and selected interatomic distances in Table 5. The results for hydrogen bond distances and angles are listed in Table 6 a-c. Raman spectra for the three rustumite samples are displayed in Figure 2. The shape of the general pattern between 1200 – 100 cm^{-1} is similar for all. Major differences are observed in the region of OH-vibrations. Rust1_LCl shows two strong bands at 3632 cm^{-1} and 3598 cm^{-1}. The latter is shifted towards lower wavenumbers at 3585 cm^{-1} in the case of Rust2_F. Only one strong band at the same position is observed for the sample Rust3_LCl_F.

Discussion

The results of our experiments confirm the correctness of the assumptions by Howie and Ilyukhin (1977) interpreting the increased electron density at the O10 site to be caused by Cl (Fig. 3). However, complete occupancy of this site by Cl is rather the exception than the rule (e.g., Kanazawa et al. 1997; Hezarkhani 2006; this study). Moreover, O11 was assumed (Howie and Ilyukhin 1977) to be OH, which is consistent with our results if we allow for substitution by F. In the present study the sites O10 and O11 (Howie and Ilyukhin 1977) have been relabelled to Cl1/OH1 and OH2/F, respectively. Cl1/OH1 is fivefold coordinated by Ca1, 2 × Ca2 and 2 × Ca3 building a square based pyramid. OH2/F is only threefold coordinated by Ca3, Ca4 and Ca5 and is adjacent to its symmetry equivalent OH2/F' (-x, y, -z +1/2). The three examined samples show variable content of monovalent anions Cl, F, OH occupying these two sites. In general depletion in Cl is reflected in shortening of the *a* axis and decrease of cell volume.

Sample Rust1_LCl (Turkey) is depleted in Cl (1.284 Cl pfu) compared to the ideal formula (Table 2). The OH2/F site is almost fully occupied by OH with minor F, while Cl1/OH1 hosts OH and Cl. The occupancy for Cl1 converged to 0.67 (Table 3a) which is consistent with the chemical analysis. OH2 and its symmetry equivalent OH2'are separated by 3.119(3) Å and are potential hydrogen bond donors and acceptors for each other. Since only one can act as an acceptor, otherwise two adjacent H sites are too close-by, two alternative hydrogen positions are present. H2b points towards OH2 leading to a hydrogen bond OH2-H2b···OH2' with a H2b···OH2'-distance of 2.19(3) Å and an OH2-H2b-OH2' angle of 154(5)° (Fig. 4). H2a points towards the anion at the Cl1/OH1 site, acting as acceptor. The distance H2a···Cl1/OH1 is 2.43(4) Å and the angle OH2-H2a-Cl1 is 141(5)° (Table 6). This indicates weaker bonding compared to OH2-H2b···OH2' (Figure 4a). The hydrogen position of OH-groups at the Cl1/OH1 site has only been derived for Rust3_LCl_F and points towards OH2/F (Figure 4c).

In sample Rust2_F (Caucasus) the Cl1/OH1 site is almost fully occupied by Cl. F and OH-groups share the OH2/F site. Regarding to hydrogen bonding, substitution of every second OH2/F site by F is favorable compared to OH-groups adjacent to each other (Figure 4b).

Sample Rust3_LCl_F (Baikal) shows severe depletion in Cl (1.00 atoms pfu) as well as high F content (0.987 atoms pfu) (Table 2). Similar to Rust2_F, OH2/F is shared by OH and F. The distance H2···F is 2.13(4) Å with an OH2-H2-F angle of 155(6)° (Table 6). The sum of the bond valences after Brown and Altermatt (1985) for F on OH2/F results in 0.78 vu. Thus F has high hydrogen-bond acceptor capacity. Cl1/OH1 hosts Cl and OH-groups similar to Rust1_LCl.

The hydrogen position H1 is at the back of the square-based pyramid centered by OH1/Cl1. H1 has the two anions at the OH2/F site as potential hydrogen bond acceptors. Our results can not rule out partial occupation of the OH1/Cl1-site by F but the arrangement of OH2/F and OH2/F' gives rise to the following prediction. Assuming an ordered situation with F on each second OH2/F site, and OH on each second OH1/Cl1 site, two possible situations result. Either H1 has OH2 as hydrogen-bond acceptor or F (Figure 4 c1 and c2). Since F is strongly underbonded, F as acceptor is most likely. The donor-acceptor distance is 3.398(10) Å and the hydrogen-bond length H1···OH2/F is 2.65(4) Å with an OH1-H1-OH2/F angle of 136(4)° (Table 6). Unique for Rust3_LCl_F is the partial occupation (0.88) of the Si3 site, which is interpreted as a hydrogarnet-type substitution $SiO_4 = (OH)_4$ (Lager et al. 1987; Galuskin et al. 2007). In the case of empty Si3 tetrahedra, O4 and O8, representing tetrahedral apices of Si3, are no longer attracted by a cationic charge in the tetrahedron center and the subsites (O4A and O8A) have elongate distances to the tetrahedron center. O4A is shifted towards the triangle Ca4, Ca5 and Ca2. The proximity of O4A to Ca2 causes displacement of Ca2 to Ca2A whenever O4A is occupied. In our model with split Ca2 (Ca2 and Ca2A) O4A bonds to Ca2A and O4 to Ca2. O8A is shifted towards Ca5, Ca4 and Ca1. The hydrogarnet-like substitution produces two similar tetrahedra next to Cl: (1) with O4A, O8A and 2 × OH2 as apices, (2) with 2 × O4A and 2 × O8A as apices (Figure 5). Instead of hydrogarnet-type substitution, the splitting of the O4 and O8 sites may also be explained by the occupation of O4A and O8A by F. However, the present data do not allow excluding neither one of these possibilities nor a combination of both.

In accordance with our X-ray experiments, the major differences in the three Raman spectra are observed in the region of OH-stretching modes. Strong bands are present in a narrow range between 3650 cm^{-1} and 3540 cm^{-1} all representing weak hydrogen bonds (Libowitzky 1999). In the range of donor-acceptor distances around 3Å the Raman-wavenumbers are closely spaced which complicates the interpretation. Furthermore, one should take into account that F and Cl have not been considered by Libowitzky (1999) as hydrogen-bond acceptors.

Both F-bearing rustumites show a strong band at 3584 cm^{-1}, which is assigned to OH2-H2···F. The band at 3632 cm^{-1} is observed for F-bearing rustumite and low-Cl rustumite and is interpreted to display the weak interaction between OH2-H2a and Cl1. Low-chlorine rustumite shows another strong band at 3598 cm^{-1}, which is most likely due to the interaction of OH2-H2···OH2. Since the fluorine content for F-bearing rustumite is not enough to occupy each second OH2/F site (< 1 F pfu) this band is also expected for F-bearing rustumite but has not been

observed. The shoulder at 3645 cm^{-1}, observed for low-Cl rustumite, may be caused by the long hydrogen bond OH1-H1···OH2/F. But this band is not observed for Rust3_LCl_F. Assuming a H-setting for the hydrogarnet-type substitution according to Lager et al. (1987) we would expect Raman-bands at higher wavenumbers which are not resolved. Although the interpretation of the Raman spectra is certainly ambiguous a slight strengthening of the hydrogen bond system due to fluorine uptake is observed. The depletion in chlorine is not obviously displayed in the Raman-spectra.

None of the hitherto reported chemical compositions of rustumite reaches the ideal chlorine content of 2 apfu, although rustumite from Northern Caucasus, studied in this paper, has 1.96 Cl pfu. Low-Cl rustumite and Cl-bearing dellaite may not be distinguished by electron microprobe analysis since they share the same Ca/Si ratio and variable Cl content (Armbruster et al. 2011). As rustumite and dellaite grow within the same mineral association (Agrell 1965, this study) the question about the formation conditions arises. A paragenesis of two Ca-silicates with the same Ca/Si ratio and similar chlorine content is rather unlikely. In sample Rust3_LCl_F (Birkhin massif) (Figure 1 c,d) replacement of dellaite by rustumite is observed along a system of cracks and micro-veins, crosscutting the preexisting dellaite-monticellite symplectites. Two reaction-series may be distinguished: (1) Dellaite – Cl-bearing dellaite – rustumite and (2) dellaite – cuspidine – rustumite + F-bearing spurrite.

Acknowledgement

We highly appreciate the constructive evaluations of two anonymous reviewers. T.A. and B.L. acknowledge support by the Swiss National Science Foundation project “Crystal Chemistry of Minerals” 200020_134617. We acknowledge receiving rustumite reference samples NMNH 119428, Smithsonian Institution, Washington, D.C. and M35011 Museum Victoria, Melbourne.

References

Agrell, S.O. (1965) Polythermal metamorphism of limestones at Kilchoan, Ardnamurchan. Mineralogical Magazine, 34, 1-15.

Armbruster, T., Lazic, B., Gfeller, F., Galuskin, E.V., Galuskina, I.O., Savelyeva, V.B., Zadov, A.E., Pertsev, N.N., and Dzierżanowsk, P. (2011) Chlorine content and crystal chemistry of dellaite from the Birkhin gabbro massif, Eastern Siberia, Russia. Mineralogical Magazine, 75, 379–394.

Bogomolov, M.A. (1970) "On Calcareous Skarns of Magmatic Stage," in Outlines of Physicochemical Petrology. Nauka,Moscow, 2, 5–14 (in Russian).

Brown, I.D. and Altermatt, D. (1985) Bond-valence parameters obtained from a systematic analysis of the Inorganic Crystal Structure Database. Acta Crystallographica, B41, 244-247.

Bruker (1999) SMART and SAINT-Plus. Versions 6.01. Bruker AXS Inc., Madison, Wisconsin, USA.

Chesnokov, B.V., Vilisov, V.A., Bushmakin, A.F., Kotlyarov, V.A., and Belogub, E.V. (1994) New minerals from a fired dump of the Chelyabinsk coal basin. "Ural'skiy Mineralogicheskiy Zbornik, 3, 3–34 (in Russian).

Dornberger-Schiff, K. and Fichtner, K. (1972) On the symmetry of od-structures consisting of equivalent layers. Kristall und Technik 7 (9) 1035–1056.

Dornberger-Schiff, K. and Organova, N.I. (1971) The symmetry of rustumite. Soviet Physics – Crystallography 16(1) 107 – 114.

Galuskin E.V., Galuskina I.O., Lazic B., Armbruster T., Zadov A.E., Krzykawski T., Banasik K., Gazeev V.M., and Pertsev N.N. (2011) Rusinovite, $Ca_{10}(Si_2O_7)_3Cl_2$: a new skarn mineral

from the Upper Chegem caldera, Kabardino-Balkaria, Northern Caucasus, Russia. European Journal of Mineralogy, 23(5), 837–844.

Galuskin, E.V., Galuskina, I.O., Stadnicka, K., Armbruster, T., and Kozanecki, M. (2007) The crystal structure of Si-deficient, OH-substituted, boron-bearing vesuvianite from the Wiluy river, Sakha-Yakutia, Russia. Canadian Mineralogist, 45, 239-248.

Galuskin, E.V., Gazeev, V.M., Lazic, B., Armbruster, T., Galuskina, I.O., Zadov, A.E., Pertsev, N.N., Wrzalik, R., Dzierżanowski, P., Gurbanov, A.G., and Bzowska, G. (2009) Chegemite $Ca_7(SiO_4)_3(OH)_2$ – a new calcium mineral of the humite-group from the Northern Caucasus, Kabardino-Balkaria, Russia. European Journal of Mineralogy, 21, 1045–1059.

Hezarkhani, A. (2006) Skarns associated with the Rize Batholith, North Eastern Turkey. Amirkabir, 16 (63-C), 93-102.

Howie R.A. and Ilyukhin V.V. (1977) Crystal structure of rustumite. Nature, 269(5625), 231–231.

Kanazawa, Y., Aoki M., and Takeda, H. (1997) Wadalite, rustumite, and spurrite from La Negra mine, Queretaro, Mexico. Bulletin Geological Survey of Japan, 48, 413–420.

Komarneni, S. (2011) Memorial of Rustum Roy, 1924-2010. American Mineralogist, 96, 1662-1663.

Lager, G., A., Armbruster, T., and Faber, J. (1987) Neutron and X-ray diffraction study of hydrogarnet $Ca_3Al_2(O_4H_4)_3$. American Mineralogist, 72, 756-765.

Lazic B., Armbruster T., Savelyeva V.B., Zadov A.E., Pertsev N.N., and Dzierzanowski P. (2011) Galuskinite, $Ca_7(SiO_4)_3(CO_3)$, a new skarn mineral from the Birkhin gabbro massif, Eastern Siberia, Russia. Mineralogical Magazine, 75(5), 2631–2648.

Libowitzky, E. (1999) Correlation of O-H stretching frequencies and O-H···O hydrogen bond lengths in minerals. Monatshefte für Chemie, 130, 1047-1059.

Nevskii, N.N., Ilyukhin,V.V., and Belov, N. V. (1979) Determination of the crystal structure of rustumite. Soviet Physics Doklady, 24, 598.

Pawlowski, J., (2008) Systematische Untersuchungen zu Korrosionsprozessen an Feuerfestmaterialien in Müll- und Biomasseverbrennungsanlagen und Einsatzmöglichkeiten von Additiven als Korrosionsinhibitoren. Dissertation, LMU München: Faculty of Geosciences, 150 p.

Sarp, H. and Burri, G. (1986) Trabzonite $Ca_4Si_3O_{10}\cdot 2H_2O$ a new hydrated silicate. Schweizerische Mineralogische Petrographische Mitteilungen, 66, 453.

Sarp, H. and Burri, G. (1987) Yeni bir mineral, trabzonit, $Ca_4Si_3O_{10}\cdot 2H_2O$. Bulletin of the Geological Society of Turkey 30, 57-60 (in Turkish).

Sheldrick, G.M. (1996) SADABS. University of Göttingen, Germany.

Sheldrick, G.M. (2008) A short history of SHELX. Acta Crystallographica, A64, 112-122.

Takechi, Y., Kusachi, I., Nakumata, Y., and Kase, K. (2000) Nickel-bearing djerfisherite in gehlenite-spurrite skarn at Kushiro, Hiroshima prefecture, Japan. Resource Geology , 50 (3), 179–184

Taner, M. (1977) Etude géologique et pétrographique de la région de Güneyce-Ikizedere (Pontides orientales, Turquie). Thése No. 1788, Université de Genève.

Zateeva, S. N., Sokol, E. V., and Sharygin, V. V. (2007) Specificity of pyrometamorphic minerals of the ellestadite group. Geology of Ore Deposits, 49 (8), 792–805.

Figure 1. (a) Back scattered electron (BSE) image of low-Cl rustumite from the Rize-batholite near Ikizdere, Eastern Turkey (Rust1_LCl). A big rustumite (Rst) grain with hydrogrossular (Hgr) inclusion is associated with defernite (Dfr), vesuvianite (Ves), dellaite (Del), spurrite (Spu), foshagite (Fsh), and killalaite (Kil). (b) BSE-.image of rustumite from the Upper Chegem Caldera, Northern Caucasus (Rust2_F). Rustumite forms lens like aggregates within a bultfonteinite (Blt) matrix. (c) Transmitted light image of low-Cl, F-bearing rustumite (Rust3_LCl_F) with crossed polarizers. Rustumite builts symplectites with monticellite (Mtc) and additional magnetite (Mgt), aggregates of clintonite (Cln) and vesuvianite. (d) Back scattered electron image of the white framed area in (c).

Figure 2. Raman spectra for Rust2_F (Caucasus) (1), Rust1_LCl (Turkey) (2) and Rust3_LCl_F (Baikal) (3).

Figure 3. The crystal structure of rustumite projected along the **a**-axis. Thin solid lines are unit cell outlines. Disilicate units are shown as red and orthosilicate units as rose tetrahedra. Disilicate units extend along **a**. Calcium atoms are displayed as yellow, oxygen as small purple, and Cl as green spheres. The black frame marks (thick solid lines) the area of the close-up in Figure 4.

Figure 4. Perspective view of hydrogen bond systems for (a) low-chlorine rustumite (Rust1_LCl) (b) F-bearing rustumite Rust2_F and (c1,c2) F-bearing, low-chlorine rustumite (Rust_3_LCl_F). Hydrogen bonds are drawn as striped cylinders. The cake diagrams display the relative amounts of monovalent anions partitioned to Cl1/OH1 left and OH2/F rigth. In (a) two hydrogen bonds are distinguished. H2a interacts with Cl1, H2b with OH2 as acceptor. For F-bearing rustumite (b) the hydrogen position points towards OH2/F. In (c) two Cl1/OH1 sites are displayed. The one in the front occupied by OH the one behind by Cl. One of the two OH2/F sites is occupied by F, which is acceptor of the hydrogen bond from H2. The hydrogen position of OH1 points towards OH2/F where it either interacts with F (c1) or OH2 (c2).

Figure 5. Detailed view of the Si3 site in Rust3_LCl_F projected along the **b**-axis with (a) and without (b) hydrogarnet-like substitution. Due to the lack of cationic charge O8 and O4 shift away from the former orthosilicate site and build two similar tetrahedra (O8A 2x OH2 2x as apices left and 2x O8A and 2x O4A as apices right). The proximity of O4A to Ca2 causes displacement of Ca2 to Ca2A whenever O4A is occupied. The green spheres represent Cl.

Table 1. Parameters for X-ray data collection and crystal-structure refinement of rustimite

Crystal data	Rust1_LCL (Turkey)	Rust2_F (Caucasus)	Rust3_LCL_F (Baikal)
Unit cell dimensions (Å)	a = 7.61428(8)	a = 7.641(5)	a = 7.5915(1)
	b = 18.5772(2)	b = 18.559(5)	b = 18.5774(4)
	c = 15.5714(2)	c = 15.537(5)	c = 15.4919(3)
	β = 104.7340(10)	β = 104.210(5)	β = 104.668(1)
Space group	$C2/c$ (No. 15)	$C2/c$ (No. 15)	$C2/c$ (No. 15)
Volume (Å^3)	2130.18(4)	2135.9(17)	2113.22(12)
Z	4	4	4
Chemical formula	$Ca_{10}(Si_2O_7)_2(SiO_4)$ $((OH)_{1.88}F_{0.12})(Cl_{1.28}(OH)_{0.72})$	$Ca_{10}(Si_2O_7)_2(SiO_4)$ $((OH)_{1.88}F_{0.87})(Cl_{1.96}(OH)_{0.04})$	$Ca_{10}(Si_2O_7)_2[(SiO_4)_{0.88}(H_4O_4)_{0.12}]$ $((OH)_{1.01}F_{0.99})(Cl_{1.00}(OH)_{1.00})$
Intensity Measurement			
Crystal shape	prism	prism	prism
Crystal size (mm)	0.4 × 0.1 × 0.1	0.06 × 0.08 × 0.1	0.07 × 0.1 × 0.1
Diffractometer	APEX II SMART	APEX II SMART	APEX II SMART
X-ray radiation	Mo Kα	Mo Kα	Mo Kα
X-ray power	50 kV 30 mA	50 kV 30 mA	50 kV 30 mA
Monochromator	Graphite	Graphite	Graphite
Temperature	293 K	293 K	293 K
Detector to sample distance	5.95 cm	5.95 cm	5.95 cm
Measurement method	Phi and Omega scans	Phi and Omega scans	Phi and Omega scans
Radiation width	0.5°	0.5°	0.5°
Time per frame	30 s	30 s	30 s
Max. θ°-range for Data collection	30.5	30.51	29.37
Index ranges	$-10 \leq h \leq 10$	$-10 \leq h \leq 9$	$-9 \leq h \leq 9$
	$-26 \leq k \leq 19$	$-26 \leq k \leq 26$	$-23 \leq k \leq 24$
	$-22 \leq l \leq 21$	$-22 \leq l \leq 20$	$-20 \leq l \leq 19$
No. of measured reflections	29084	21837	11124
No. of unique reflections	3257	3263	2534
No. of observed reflections ($I > 2\sigma(I)$)	2988	2976	2204
Refinement of the structure			
No. of parameters used in refinement	178	169	195
R_{int}	0.028	0.0371	0.0255
R_σ	0.0166	0.0311	0.0240
$R1$, $I > 2\sigma(I)$	0.0205	0.0295	0.0243
$R1$ all Data	0.0229	0.0344	0.0303
$wR2$ on (F^2)	0.0541	0.0721	0.0630
$GooF$	1.053	1.057	1.066
$\Delta\rho_{min}$ (-e$^-$ Å^{-3})	-0.68 close to Si3	-0.59 close to Si1	-0.56 close to O4A
$\Delta\rho_{max}$ (e$^-$ Å^{-3})	0.78 close to Ca2	1.08 close to OH10	0.41 close to H2

Table 2 Chemical compositions for studied rustumites

	Rust1_LCl (Rize) mean of 19			Rust2_F (Chegem) mean of 40			Rust3 LCl_F* (Birkhin) mean of 17		
	wt. %	s.d.	Range	wt. %	s.d.	Range	wt. %	s.d.	Range

SiO_2	32.46	0.14	32.21-32.77	31.94	0.31	31.31-32.62	31.35	0.41	30.65-32.03
Fe_2O_3	0.17	0.06	0.08-0.31	n.d.			n.d		
MgO	0.15	0.01	0.12-0.17	n.d.			0.03	0.01	0.01-0.05
CaO	60.95	0.36	60.32-61.54	59.60	0.44	59.05-60.79	60.05	0.92	58.30-61.66
MnO	0.06	0.05	0-0.16	n.d.			n.d		
F	0.25	0.17	0-0.51	1.76	0.25	1.42-2.28	2.01	0.32	1.35-2.45
Cl	4.96	0.10	4.66-5.11	7.38	0.32	6.90-7.99	3.80	0.12	3.59-4.00
H_2O^{**}	2.55			1.12			1.94		
H_2O^{***}							0.51		
-O=F+Cl	1.22			2.41			1.7		
Total	100.38			99.40			97.99		

Atoms p.f.u. (Rust1_LCl and Rust2_F normalized to 15 cations, Rust3_LCl_F normalized to 10 cations on X)			
Ca	9.979	9.999	9.993
Mn^{2+}	0.008		
Mg	0.034		0.007
Σ X	**10.021**	**9.999**	**10**
Si	4.959	5.001	4.868
Fe^{3+} ****	0.02		n.d.
$4H^+$			0.131
Σ Z	**4.979**	**5.001**	**5**
F	0.121	0.873	0.987
Cl	1.284	1.958	1
OH	2.599	1.17	2.013

* Chemical data measured on four single crystals of Rust3_LCl_F after single-crystal X-ray experiments

** H_2O calculated to obtain (OH+F+Cl) = 4 pfu

*** H_2O calculated for hydrogarnet-type substitution

**** Fe assumed to be 3^+ due to oxydizing conditions

Table 3a Atom coordinates, U_{eq} (Å^2) values for Rust1_LCL

Site	Atom	x	y	z	U_{eq}	Occupancy
Ca1	Ca	0.25832(4)	0.350692(19)	0.250154(19)	0.01387(7)	1
Ca2	Ca	0.44126(4)	0.302119(17)	0.62064(2)	0.01440(7)	1
Ca3	Ca	0.57602(4)	0.206694(17)	0.40467(2)	0.01387(7)	1
Ca4	Ca	0.32996(4)	0.023226(17)	0.40168(2)	0.01268(7)	1
Ca5	Ca	0.31132(4)	0.513971(17)	0.39681(2)	0.01269(7)	1
Si1	Si	0.44260(5)	0.63248(2)	0.56131(3)	0.00800(8)	1
Si2	Si	0.36933(5)	0.13390(2)	0.56369(3)	0.00795(8)	1
Si3	Si	0.5	0.52703(3)	0.25	0.01101(11)	1
O1	O	0.33373(15)	0.37864(7)	0.41664(8)	0.0169(2)	1
O2	O	0.47860(16)	0.17637(6)	0.65077(8)	0.0165(2)	1
O3	O	0.43122(15)	0.05230(6)	0.55592(8)	0.0147(2)	1
O4	O	0.46214(14)	0.57598(6)	0.15897(7)	0.0124(2)	1
O5	O	0.34738(16)	0.17677(8)	0.47193(8)	0.0219(3)	1
O6	O	0.37689(15)	0.68737(6)	0.47854(7)	0.0142(2)	1
O7	O	0.42280(15)	0.32696(6)	0.14990(7)	0.0132(2)	1
O8	O	0.31773(15)	0.47813(6)	0.24725(7)	0.0147(2)	1
O9	O	0.36633(16)	0.44762(6)	0.04238(7)	0.0159(2)	1
Cl1	Cl	0.23505(11)	0.29647(5)	0.74531(5)	0.0121(2)	0.668(4)
OH1	O	0.2693(9)	0.2871(4)	0.7388(4)	0.0121(2)	0.332(4)
OH2	O	0.05764(18)	0.58852(7)	0.35353(9)	0.0215(3)	1
H2a*	H	0.084(8)	0.605(3)	0.301(3)	0.050	0.5
H2b*	H	0.011(8)	0.573(3)	0.2909(17)	0.050	0.5

* Occupancy restraint to 0.5, U_{iso} is fixed

Table 3b Atom coordinates, U_{eq} (Å^2) values Rust2_F

Site	Atom	x	y	z	U_{eq}	Occupancy
Ca1	Ca	0.25798(8)	0.35393(3)	0.24957(4)	0.01027(10)	1
Ca2	Ca	0.43775(15)	0.30194(3)	0.61596(4)	0.01071(12)	1
Ca3	Ca	0.57805(14)	0.20586(3)	0.40290(4)	0.01077(12)	1
Ca4	Ca	0.33037(14)	0.02442(3)	0.40105(4)	0.01022(12)	1
Ca5	Ca	0.31089(14)	0.51572(3)	0.39654(4)	0.01050(13)	1
Si1	Si	0.44245(12)	0.63185(5)	0.56208(6)	0.0091(2)	1
Si2	Si	0.37051(12)	0.13369(5)	0.56444(6)	0.0090(2)	1
Si3	Si	0.5	0.52862(6)	0.25	0.0082(2)	1
O1	O	0.3328(5)	0.37894(12)	0.41699(15)	0.0183(4)	1
O2	O	0.4770(4)	0.17640(12)	0.65165(15)	0.0152(6)	1
O3	O	0.4319(4)	0.05197(12)	0.55667(17)	0.0148(6)	1
O4	O	0.4619(5)	0.57715(10)	0.15820(13)	0.0099(4)	1
O5	O	0.3500(6)	0.17740(13)	0.47332(15)	0.0177(5)	1
O6	O	0.3756(6)	0.68675(11)	0.47952(13)	0.0129(5)	1
O7	O	0.4253(4)	0.32812(12)	0.15085(14)	0.0137(6)	1
O8	O	0.3188(3)	0.47948(10)	0.24750(19)	0.0114(4)	1
O9	O	0.3691(5)	0.44801(12)	0.04318(15)	0.0167(7)	1
Cl1	Cl	0.23802(11)	0.29671(3)	0.74573(5)	0.01181(12)	1
OH2*	O	0.0586(5)	0.58779(10)	0.35717(14)	0.0170(4)	0.56
F*	O	0.0586(5)	0.58779(10)	0.35717(14)	0.0170(4)	0.44
H2**	H	0.0032	0.5753	0.3003		0.56

*Occupancies constrained based on chemical analysis

**Unrefined H-position based on a peak of 0.47 electrons in the difference Fourier-map

Table 3c Atom coordinates, U_{eq} (Å^2) values for Rust3_LCL_F

Site	Atom	x	y	z	U_{eq}	Occupancy
Ca1	Ca	0.25750(6)	0.34755(3)	0.25122(3)	0.01576(13)	1
Ca2	Ca	0.05738(11)	0.19741(5)	0.37627(8)	0.01366(18)	0.876(4)
Ca2A*	Ca	0.0682(9)	0.2087(4)	0.3999(4)	0.0107(16)	0.124(4)
Ca3	Ca	0.57526(6)	0.20592(3)	0.40091(3)	0.01491(12)	1
Ca4	Ca	0.32951(6)	0.02325(3)	0.40035(3)	0.01281(12)	1
Ca5	Ca	0.31077(6)	0.51402(3)	0.39670(3)	0.01239(12)	1
Si1	Si	0.44131(8)	0.63282(3)	0.56080(4)	0.00843(14)	1
Si2	Si	0.36948(8)	0.13400(3)	0.56307(4)	0.00859(14)	1
Si3*	Si	0.5000	0.52578(6)	0.2500	0.0111(3)	0.876(4)
O1	O	0.3347(2)	0.37761(9)	0.41829(11)	0.0178(4)	1
O2	O	0.4779(2)	0.17673(9)	0.65060(11)	0.0157(4)	1
O3	O	0.4305(2)	0.05234(8)	0.55589(11)	0.0145(3)	1
O4	O	0.4623(3)	0.57562(11)	0.15895(13)	0.0182(5)	1
O4A*	O	0.465(3)	0.5906(11)	0.1340(13)	0.020	0.124(4)
O5	O	0.3497(2)	0.17680(10)	0.47095(12)	0.0226(4)	1
O6	O	0.3740(2)	0.68675(9)	0.47707(11)	0.0171(4)	1
O7	O	0.4229(2)	0.32617(8)	0.14988(10)	0.0131(3)	1
O8	O	0.3170(3)	0.47661(10)	0.24771(12)	0.0123(4)	0.876(4)
O8A*	O	0.228(3)	0.4644(10)	0.2488(12)	0.031(5)	0.124(4)
O9	O	0.3663(2)	0.44751(9)	0.04316(11)	0.0165(4)	1
OH1	O	0.2669(12)	0.2882(6)	0.7418(7)	0.0134(6)	0.504(6)
Cl1	Cl	0.2363(4)	0.29711(18)	0.7453(2)	0.0134(6)	0.496(6)
OH2	O	0.0561(2)	0.58843(9)	0.35092(11)	0.0215(6)	0.53(3)
F	F	0.0561(2)	0.58843(9)	0.35092(11)	0.0215(6)	0.47(3)
H1**	H	0.218(6)	0.3348(17)	0.746(3)	0.007(15)	0.504(6)
H2**	H	0.032(12)	0.574(4)	0.2895(19)	0.08(3)	0.53(3)

*refined occupancies due to hydrogarnet-type substitution

** U_{iso} has been refined

Table 4a Anisotropic displacement parameters U_{ij} for Rust1_LCl (deposited material).

Site	U_{11}	U_{22}	U_{33}	U_{23}	U_{13}	U_{12}
Ca1	0.01118(13)	0.02046(16)	0.00972(13)	-0.00253(10)	0.00221(10)	-0.00015(11)
Ca2	0.01266(14)	0.01100(14)	0.02074(15)	0.00259(11)	0.00645(11)	0.00091(11)
Ca3	0.01230(14)	0.01098(14)	0.01889(15)	0.00278(11)	0.00499(11)	0.00043(10)
Ca4	0.01006(13)	0.01582(15)	0.01157(13)	0.00035(11)	0.00167(10)	0.00160(11)
Ca5	0.01448(14)	0.01223(14)	0.01274(13)	-0.00173(10)	0.00599(11)	-0.00279(11)
Si1	0.00752(17)	0.00848(17)	0.00823(16)	-0.00007(13)	0.00244(13)	0.00028(13)
Si2	0.00719(17)	0.00870(18)	0.00785(16)	-0.00017(13)	0.00172(13)	0.00018(13)
Si3	0.0125(3)	0.0107(3)	0.0098(2)	0.000	0.0027(2)	0.000
O1	0.0085(5)	0.0220(6)	0.0215(5)	0.0060(5)	0.0060(4)	0.0024(4)
O2	0.0179(5)	0.0137(5)	0.0143(5)	-0.0039(4)	-0.0025(4)	-0.0001(4)
O3	0.0142(5)	0.0106(5)	0.0193(5)	-0.0035(4)	0.0044(4)	0.0021(4)
O4	0.0133(5)	0.0108(5)	0.0129(5)	0.0006(4)	0.0030(4)	0.0012(4)
O5	0.0134(5)	0.0351(7)	0.0171(5)	0.0143(5)	0.0039(4)	0.0008(5)
O6	0.0137(5)	0.0162(5)	0.0128(5)	0.0051(4)	0.0034(4)	0.0028(4)
O7	0.0168(5)	0.0130(5)	0.0112(5)	0.0015(4)	0.0060(4)	-0.0012(4)
O8	0.0165(5)	0.0151(5)	0.0124(5)	-0.0003(4)	0.0035(4)	-0.0030(4)
O9	0.0222(6)	0.0125(5)	0.0133(5)	0.0022(4)	0.0051(4)	0.0060(4)
Cl1	0.0111(4)	0.0133(4)	0.0122(3)	0.0004(2)	0.0036(2)	0.0004(2)
OH1	0.0111(4)	0.0133(4)	0.0122(3)	0.0004(2)	0.0036(2)	0.0004(2)
OH2	0.0254(6)	0.0163(6)	0.0238(6)	0.0008(5)	0.0080(5)	0.0013(5)

Table 4b Anisotropic displacement parameters U_{ij} for Rust2_F (deposited material).

Site	U_{11}	U_{22}	U_{33}	U_{23}	U_{13}	U_{12}
Ca1	0.0129(4)	0.0088(2)	0.0092(2)	-0.0010(2)	0.0027(5)	-0.0006(2)
Ca2	0.0101(3)	0.0092(2)	0.0137(2)	0.0025(2)	0.0045(3)	0.0010(3)
Ca3	0.0094(3)	0.0092(2)	0.0138(2)	0.0028(2)	0.0029(4)	0.0005(3)
Ca4	0.0087(3)	0.0126(3)	0.0090(2)	0.0009(2)	0.0016(4)	0.0008(3)
Ca5	0.0130(4)	0.0099(3)	0.0094(2)	-0.00079(19)	0.0043(4)	-0.0008(3)
Si1	0.0128(6)	0.0070(3)	0.0076(4)	0.0001(3)	0.0028(3)	0.0000(3)
Si2	0.0119(6)	0.0074(4)	0.0071(4)	-0.0001(3)	0.0012(3)	-0.0003(3)
Si3	0.0088(5)	0.0077(4)	0.0077(4)	0.000	0.0011(6)	0.000
O1	0.0122(11)	0.0218(11)	0.0215(11)	0.0063(8)	0.0054(14)	0.0030(12)
O2	0.0187(17)	0.0113(9)	0.0127(10)	-0.0042(8)	-0.0019(11)	-0.0003(11)
O3	0.0166(18)	0.0097(9)	0.0184(11)	-0.0027(8)	0.0051(11)	0.0032(10)
O4	0.0104(12)	0.0081(9)	0.0114(9)	-0.0003(7)	0.0031(12)	0.0002(12)
O5	0.0110(14)	0.0275(12)	0.0149(10)	0.0117(9)	0.0036(13)	-0.0001(14)
O6	0.0133(14)	0.0141(9)	0.0108(9)	0.0043(7)	0.0019(13)	0.0022(12)
O7	0.0224(18)	0.0094(9)	0.0099(9)	0.0007(7)	0.0053(11)	-0.0005(11)
O8	0.0145(10)	0.0099(9)	0.0098(9)	-0.0013(10)	0.0033(10)	-0.0026(8)
O9	0.029(2)	0.0094(9)	0.0120(11)	0.0019(8)	0.0058(12)	0.0055(11)
Cl1	0.0120(4)	0.0114(2)	0.0115(3)	0.0008(3)	0.0019(5)	0.0002(3)
OH2/F	0.0152(12)	0.0104(8)	0.0274(11)	0.0045(7)	0.0091(14)	0.0028(13)

Table 4c Anisotropic displacement parameters U_{ij} for low-Cl rustumite (deposited material).

Site	U_{11}	U_{22}	U_{33}	U_{23}	U_{13}	U_{12}
Ca1	0.0113(2)	0.0257(3)	0.0100(2)	-0.00274(18)	0.00221(17)	0.00139(19)
Ca2	0.0134(3)	0.0094(4)	0.0192(5)	0.0018(3)	0.0060(3)	0.0007(2)
Ca3	0.0137(2)	0.0100(2)	0.0216(3)	0.00354(18)	0.00538(19)	0.00085(18)
Ca4	0.0110(2)	0.0145(3)	0.0132(2)	0.00132(17)	0.00343(17)	0.00122(18)
Ca5	0.0139(2)	0.0119(2)	0.0124(2)	-0.00133(17)	0.00523(18)	-0.00198(18)
Si1	0.0082(3)	0.0086(3)	0.0086(3)	-0.0001(2)	0.0023(2)	0.0002(2)
Si2	0.0080(3)	0.0087(3)	0.0090(3)	-0.0005(2)	0.0021(2)	0.0002(2)
Si3	0.0121(5)	0.0108(6)	0.0097(5)	0.000	0.0019(4)	0.000
O1	0.0088(8)	0.0237(10)	0.0219(9)	0.0038(7)	0.0060(6)	0.0015(7)
O2	0.0164(8)	0.0142(9)	0.0142(8)	-0.0036(6)	-0.0006(6)	-0.0005(7)
O3	0.0144(8)	0.0106(8)	0.0187(8)	-0.0030(6)	0.0048(7)	0.0015(6)
O4	0.0206(9)	0.0169(11)	0.0175(11)	0.0010(7)	0.0057(9)	-0.0002(8)
O5	0.0146(9)	0.0337(11)	0.0196(9)	0.0135(8)	0.0047(7)	0.0024(8)
O6	0.0158(8)	0.0198(9)	0.0155(8)	0.0075(7)	0.0036(7)	0.0027(7)
O7	0.0172(8)	0.0113(8)	0.0123(8)	0.0009(6)	0.0066(6)	-0.0004(6)
O8	0.0119(10)	0.0138(10)	0.0109(9)	-0.0001(7)	0.0024(7)	-0.0004(8)
O9	0.0225(9)	0.0125(9)	0.0154(8)	0.0027(6)	0.0060(7)	0.0063(7)
OH	0.0123(11)	0.0123(12)	0.0158(6)	0.0006(6)	0.0041(7)	0.0021(7)
Cl1	0.0123(11)	0.0123(12)	0.0158(6)	0.0006(6)	0.0041(7)	0.0021(7)
OH	0.0236(10)	0.0158(10)	0.0260(10)	0.0004(7)	0.0080(7)	0.0010(7)
F	0.0236(10)	0.0158(10)	0.0260(10)	0.0004(7)	0.0080(7)	0.0010(7)

Table 5 Selected interatomic distances (Å)

Site1	Site2	Rust1_LCl	Rust2_F	Rust3_LCl_F
Ca1	O1	2.5618(13)	2.565(2)	2.5663(18)
	O2	2.3468(12)	2.374(3)	2.3374(16)
	O2	2.7024(12)	2.693(3)	2.6621(17)
	O7	2.2791(11)	2.276(3)	2.2799(16)
	O7	2.5670(12)	2.577(3)	2.5513(16)
	O8	2.4128(12)	2.378(2)	2.443(2)
Mean		**2.478**	**2.477**	**2.473**
	Cl1	2.7349(9)	2.7967(10)	2.688(3)
	OH1	2.578(7)		2.534(12)
	O8A			2.182(19)
Ca2	O2	2.3855(12)	2.397(2)	2.3781(18)
	O4	2.3369(11)	2.333(2)	2.323(2)
	O5	2.3346(13)	2.326(4)	2.3611(19)
	O6	2.3298(11)	2.306(4)	2.3491(19)
Mean		**2.347**	**2.341**	**2.353**
	Cl1	2.7920(8)	2.8551(17)	2.739(3)
	Cl1	2.7975(9)	2.8133(15)	2.750(3)
	OH1	2.531(6)		2.536(10)
	OH1	2.696(7)		2.636(11)
Ca2A	O2			2.264(7)
	O4A			2.25(2)
	O5			2.222(7)
	O5			2.878(7)
	O6			2.159(7)
Mean				**2.355**
	Cl1			2.994(7)
	Cl1			3.007(7)
	OH1			2.789(12)
	OH1			2.898(12)
Ca3	O5	2.3161(12)	2.334(4)	2.3114(17)
	O6	2.3151(12)	2.320(4)	2.3036(16)
	O6	2.6414(12)	2.668(2)	2.7071(18)
	O7	2.3911(12)	2.416(2)	2.3696(16)
Mean		**2.416**	**2.435**	**2.423**
	Cl1	2.8729(9)	2.9034(16)	2.831(3)
	Cl1	3.0259(8)	2.9875(14)	2.967(3)
	OH1	2.989(7)		2.956(10)
	OH2/F	2.3273(13)	2.297(2)	2.3083(17)
Ca4	O3	2.2585(11)	2.271(3)	2.2641(16)
	O3	2.3902(12)	2.406(3)	2.3979(17)
	O4	2.3939(11)	2.405(4)	2.381(2)
	O5	3.0457(15)	3.043(3)	3.045(2)

	O8	2.4531(12)	2.455(3)	2.4408(18)
	O9	2.3723(11)	2.394(3)	2.3694(16)
Mean		**2.486**	**2.496**	**2.483**
	OH2/F	2.3875(13)	2.340(3)	2.3832(16)
	O4A			2.50(2)
	O8A			2.493(18)
Ca5	O1	2.5334(13)	2.559(2)	2.5567(18)
	O3	2.4818(12)	2.492(3)	2.4687(17)
	O4	2.4123(11)	2.400(4)	2.402(2)
	O8	2.4346(11)	2.426(3)	2.4223(19)
	O9	2.3107(11)	2.312(2)	2.3135(17)
	O9	2.6941(13)	2.704(4)	2.6922(18)
Mean		**2.478**	**2.456**	**2.476**
	OH2/F	2.3326(13)	2.302(3)	2.3357(17)
	O4A			2.36(2)
	O8A			2.401(18)
Si1	O1	1.6624(11)	1.680(4)	1.6598(16)
	O6	1.6197(12)	1.620(2)	1.6161(17)
	O7	1.6122(11)	1.600(2)	1.6131(16)
	O9	1.5973(12)	1.586(3)	1.5961(17)
Mean		**1.623**	**1.622**	**1.621**
Si2	O1	1.6672(11)	1.665(4)	1.6611(16)
	O2	1.6060(12)	1.608(3)	1.6066(16)
	O3	1.6010(12)	1.601(2)	1.5982(16)
	O5	1.6070(12)	1.606(2)	1.6071(17)
Mean		**1.620**	**1.620**	**1.618**
Si3	O4 2 ×	1.6466(11)	1.651(2)	1.651(2)
	O8 2 ×	1.6502(12)	1.650(2)	1.656(2)
Mean		**1.648**	**1.651**	**1.654**
Si3 (Vac.)	O4A 2 ×			2.124(18)
	O8A 2 ×			2.35(2)
H1	OH1			0.95(2)
H2a	OH2	0.95(2)		0.96(2)
H2b	OH2	0.992(19)		

Table 6 Hydrogen bonds for studied rustumites

d(D···A)	D-H	H···A	D···A	<(DHA)
Rust1_LCl				
OH2-H2a···Cl1	0.95(2)	2.43(4)	3.2230(15)	141(5)
OH2-H2b···OH2	0.992(19)	2.19(3)	3.119(3)	154(5)
Rust2_F				
OH2···Cl1	-	-	3.242(3)	-
OH2/F···OH2/F*	0.91	2.39	3.229(4)	154
Rust3_LCl_F				
OH1-H1···OH2	0.95(2)	2.65(4)	3.398(10)	136(4)
OH2-H2···OH2/F	0.96(2)	2.13(4)	3.026(3)	155(6)

* Unrefined H-position based on a peak of 0.47 electrons in the difference Fourier-map

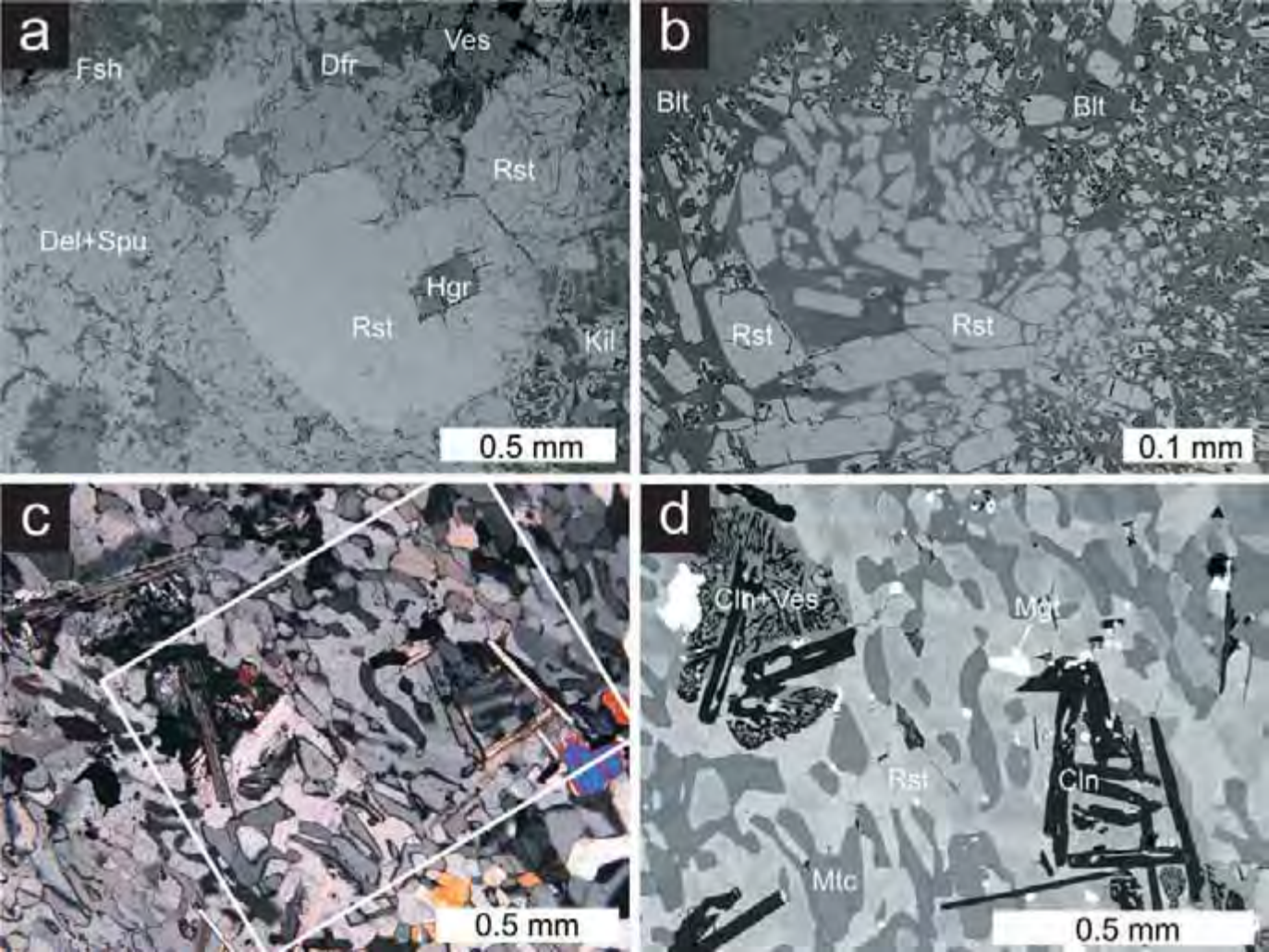
a
Fsh
Dfr
Ves
Rst
Del+Spu
Hgr
Rst
Kil
0.5 mm
b
Blt
Blt
Rst
Rst
0.1 mm
c
0.5 mm
d
Cln+Ves
Mgt
Rst
Cln
Mtc
0.5 mm

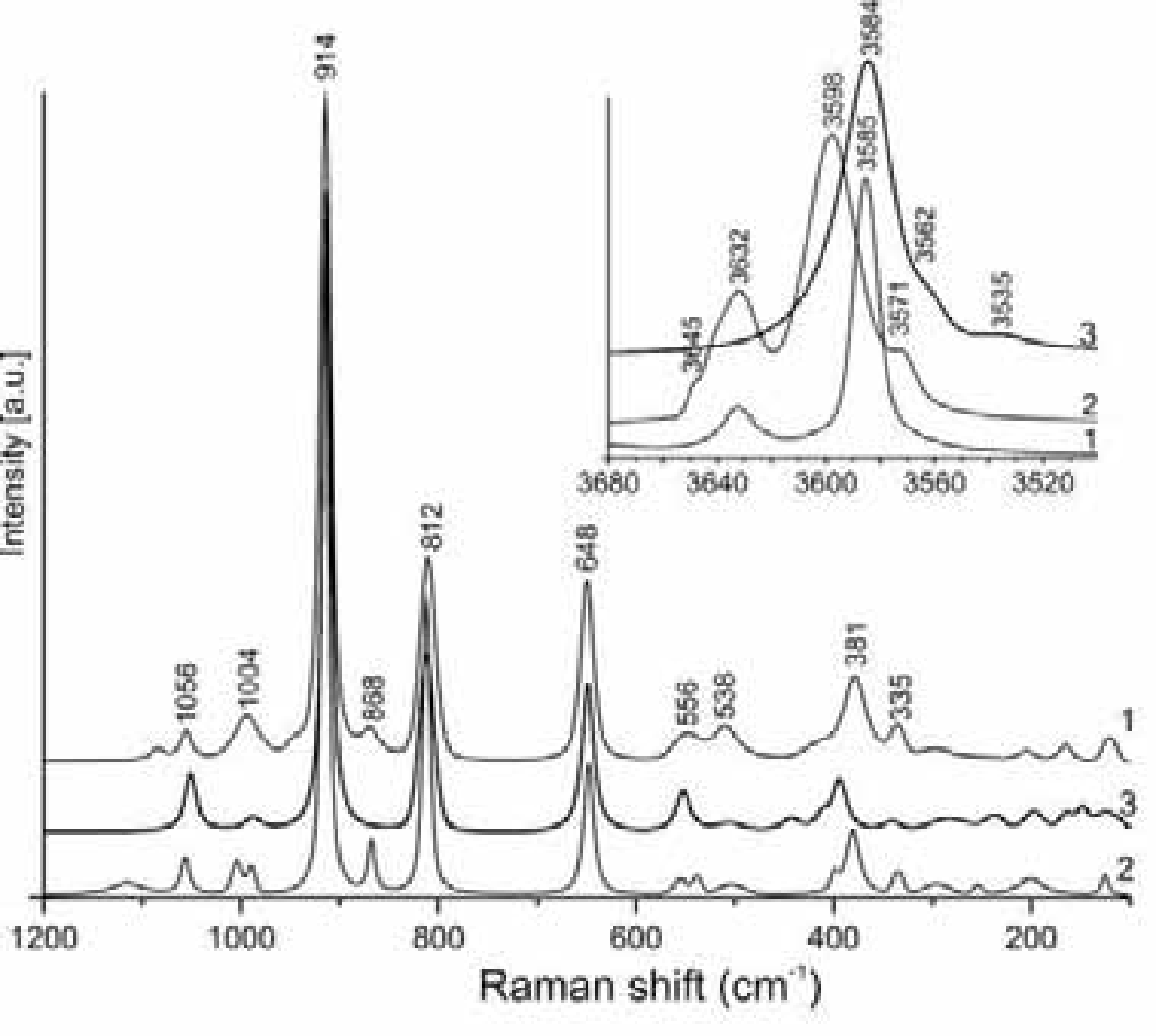
Intensity [a.u.]
914
1056
1004
868
812
648
556
538
381
335
1
3
2
1200
1000
800
600
400
200
Raman shift (cm-1)
3684
3598
3585
3632
3645
3571
3562
3535
3680
3640
3600
3560
3520

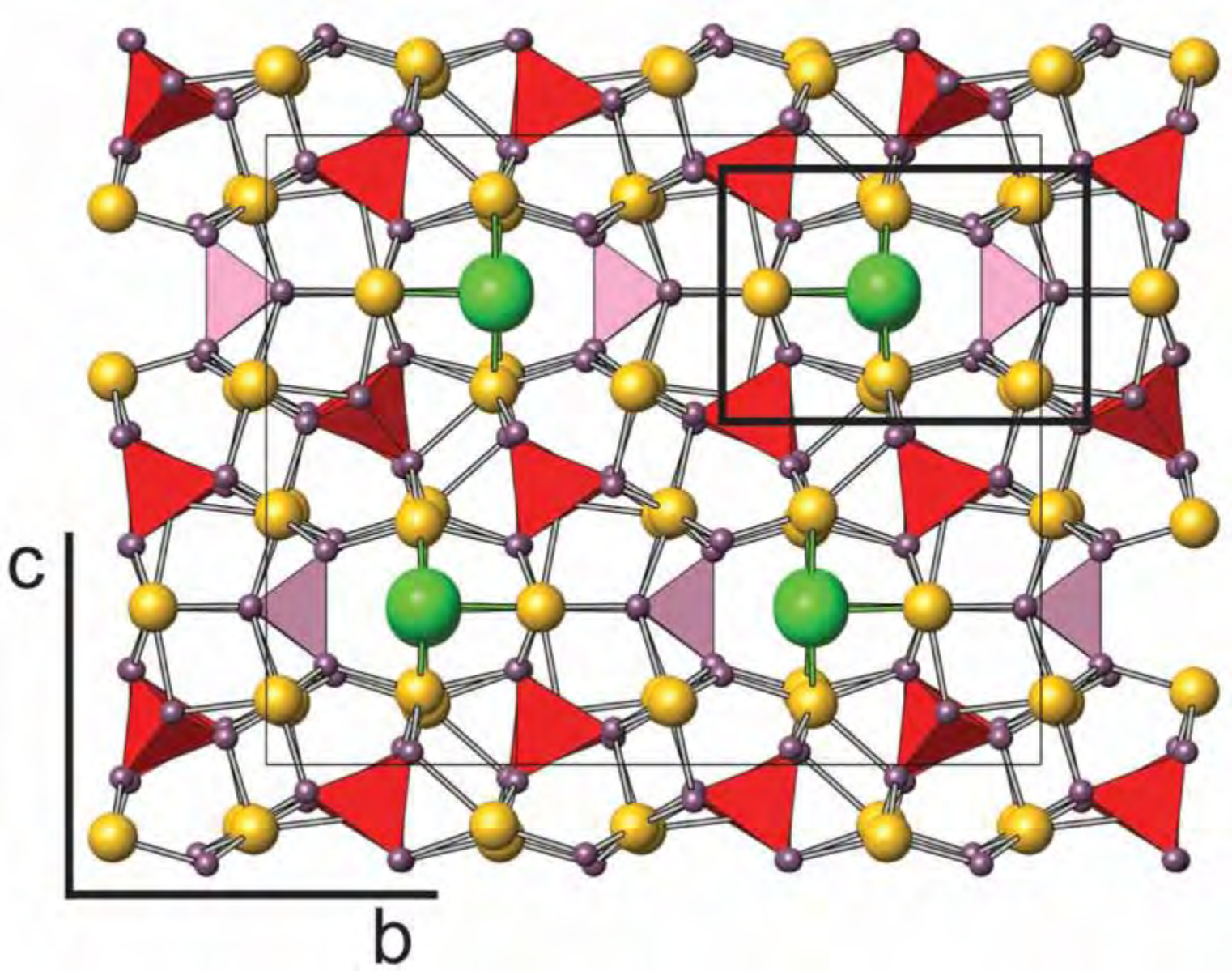
c
b

(a)

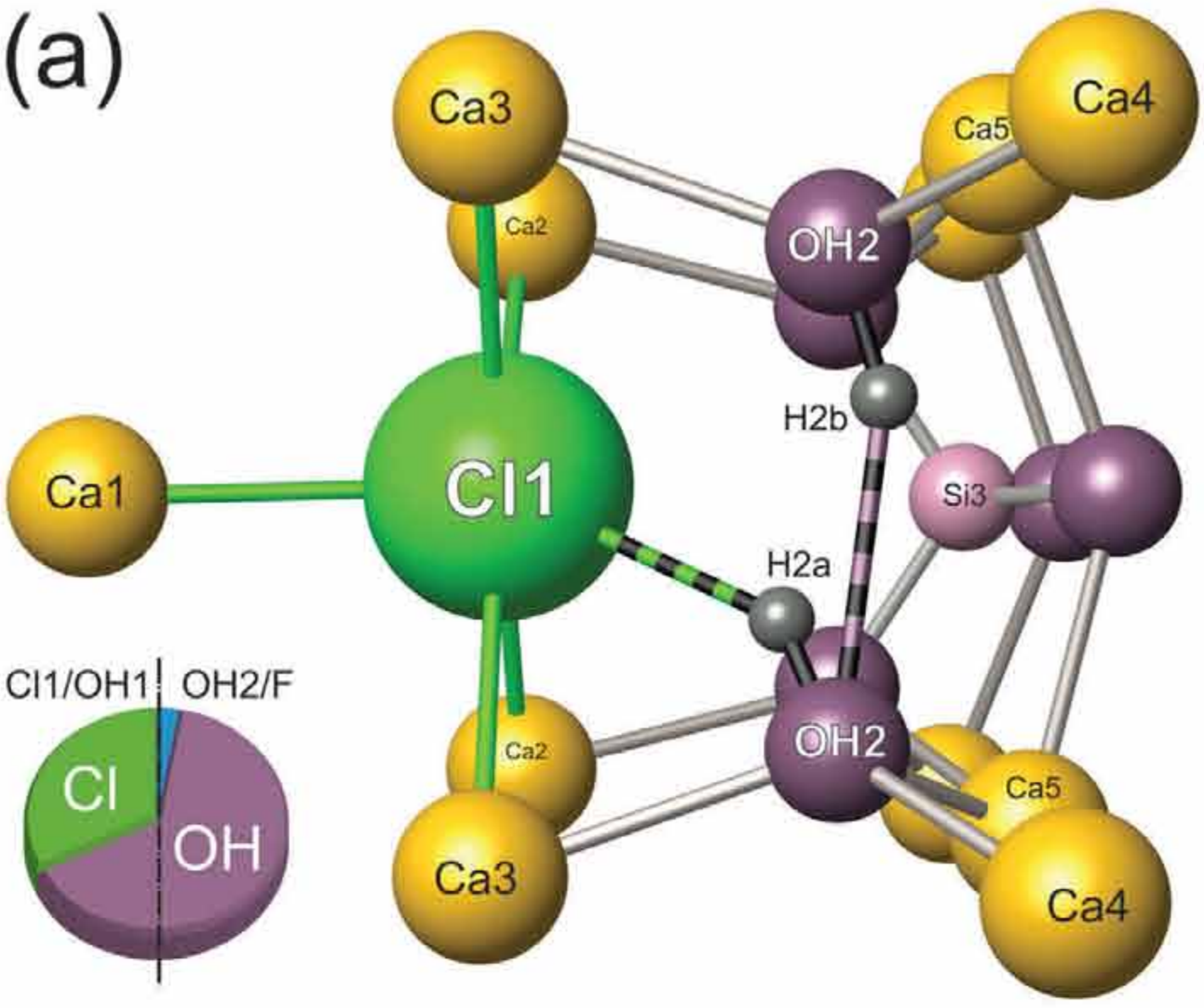
Ca3
Ca4
Ca5
Ca2
OH2
H2b
Ca1
Cl1
Si3
H2a
Cl1/OH1
OH2/F
Cl
OH
Ca2
OH2
Ca5
Ca3
Ca4

(b)

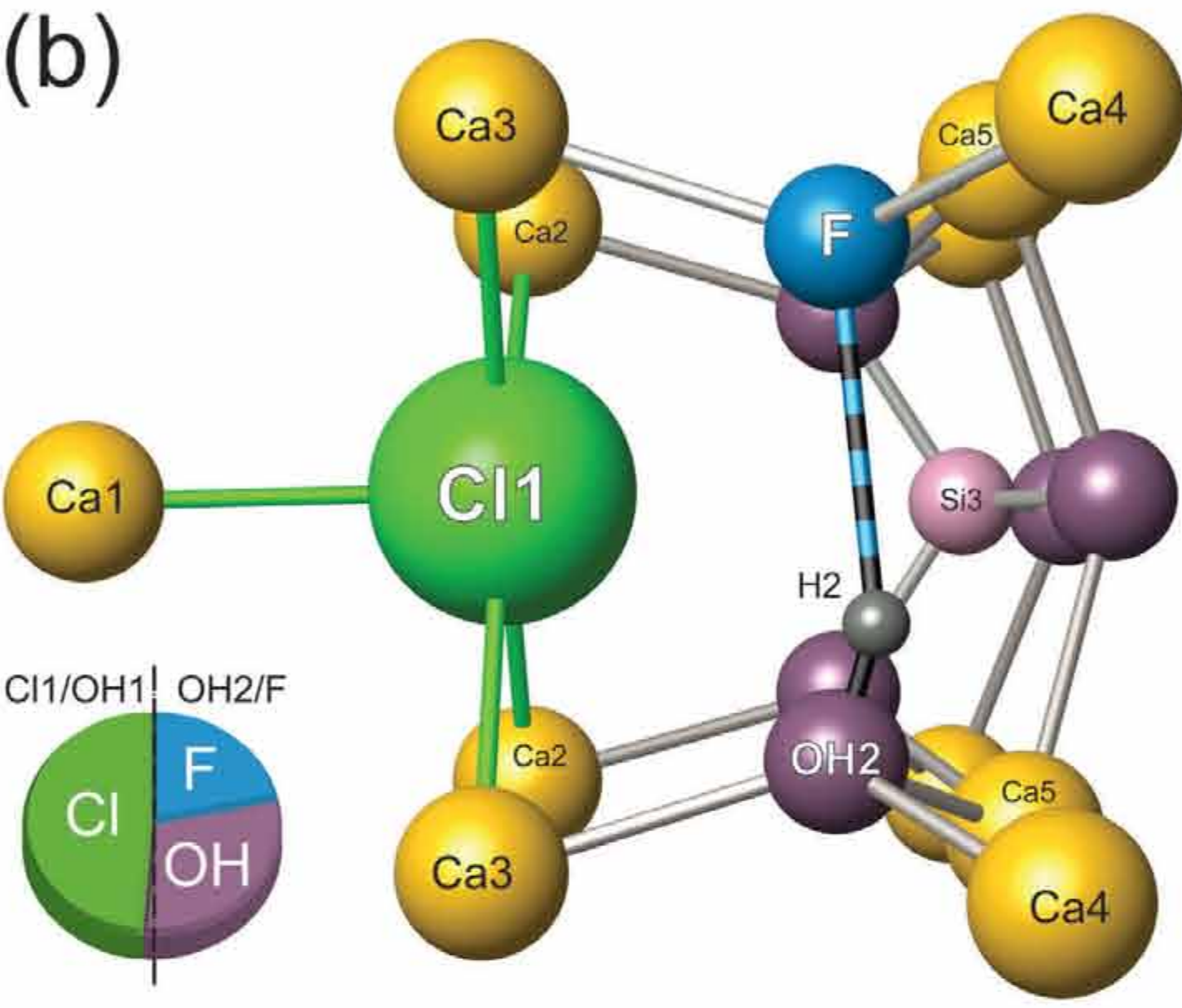
Ca3
Ca4
Ca5
Ca2
F
Ca1
Cl1
Si3
H2
Cl1/OH1
OH2/F
Cl
F
OH
Ca2
OH2
Ca5
Ca3
Ca4

(c1)

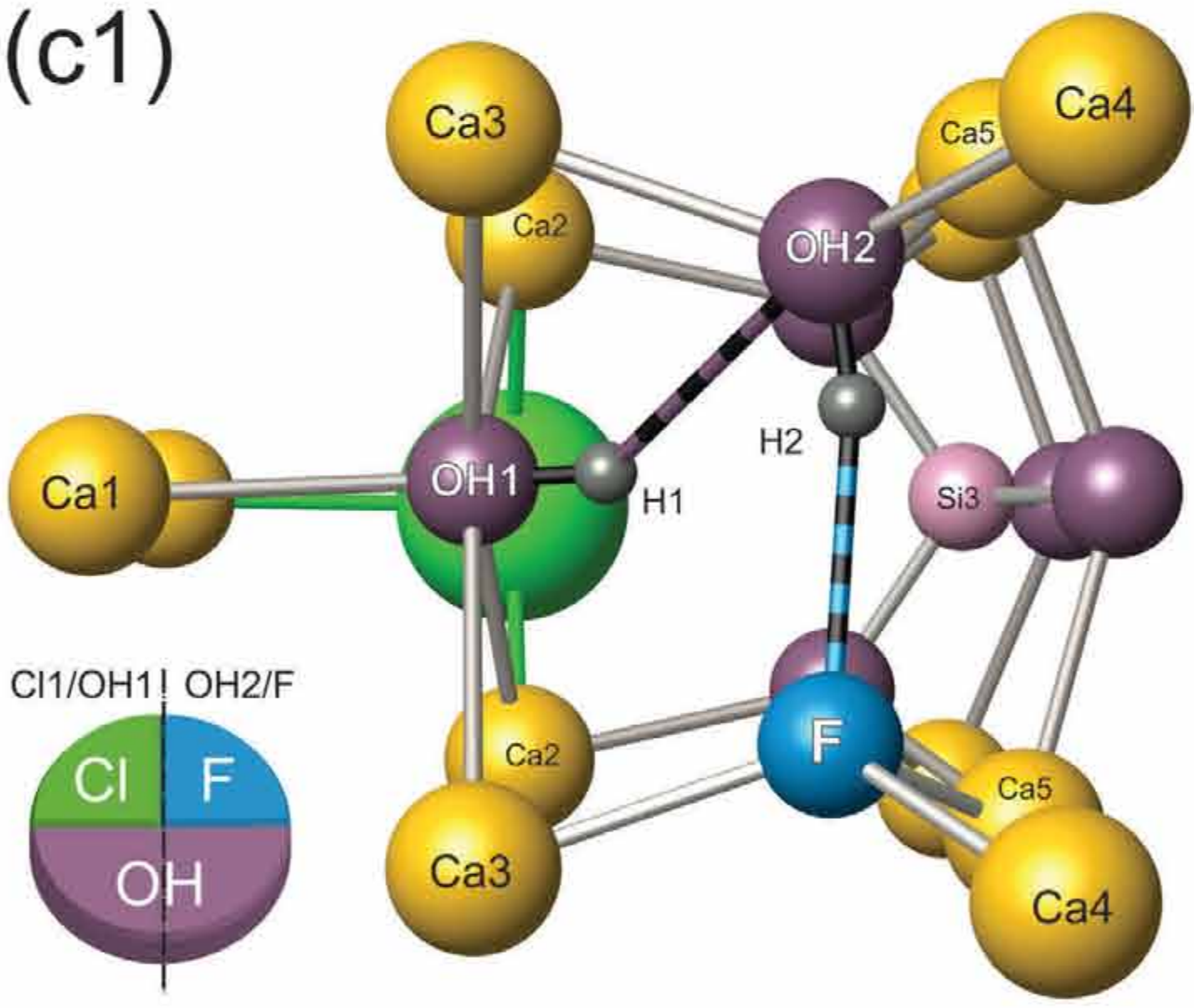
Ca3
Ca4
Ca5
Ca2
OH2
H2
Ca1
OH1
H1
Si3
Cl1/OH1
OH2/F
Cl
F
OH
Ca2
F
Ca5
Ca3
Ca4

(c2)

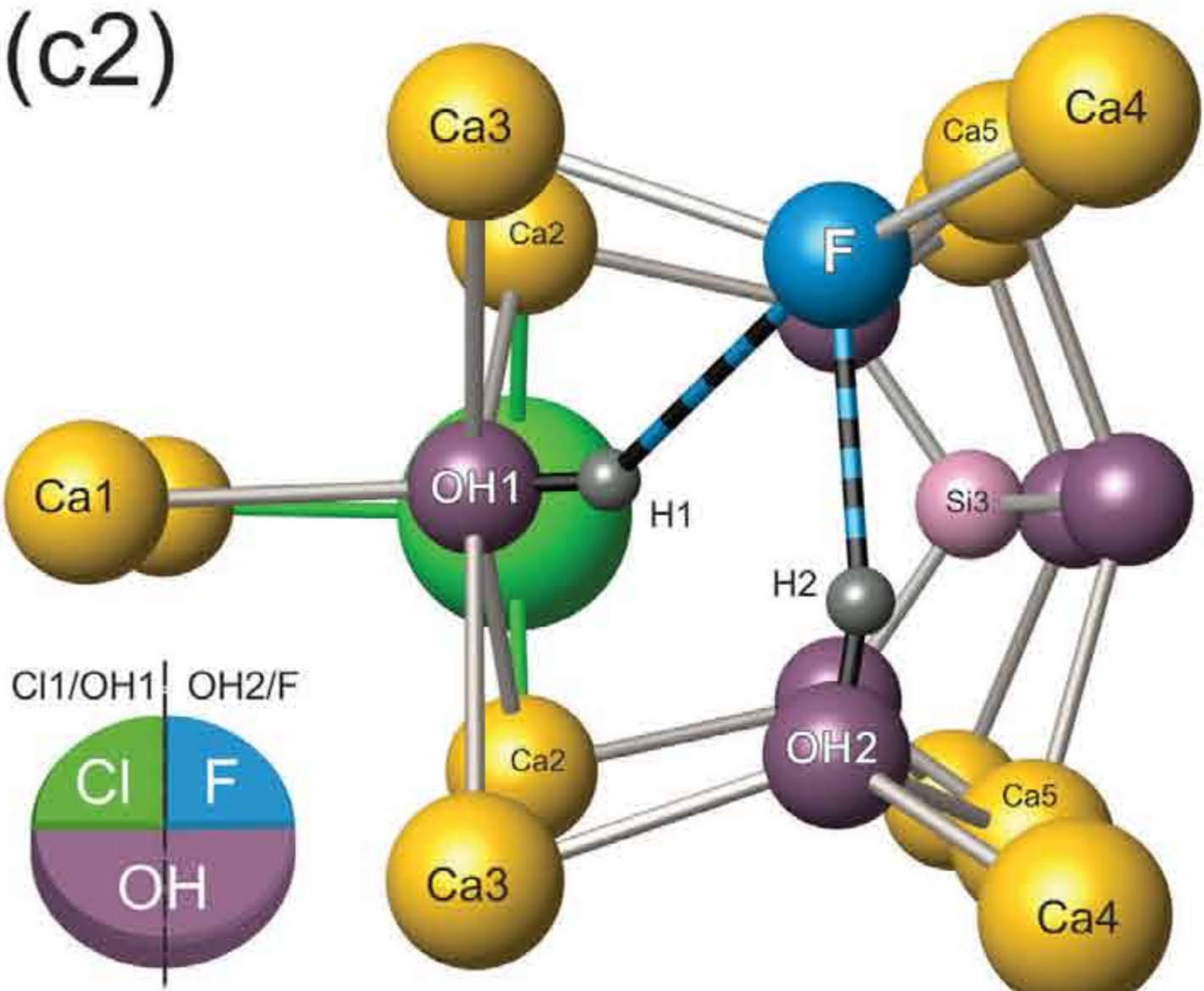
Ca3
Ca4
Ca5
Ca2
F
Ca1
OH1
H1
Si3
H2
Cl1/OH1
OH2/F
Cl
F
OH
Ca2
OH2
Ca5
Ca3
Ca4

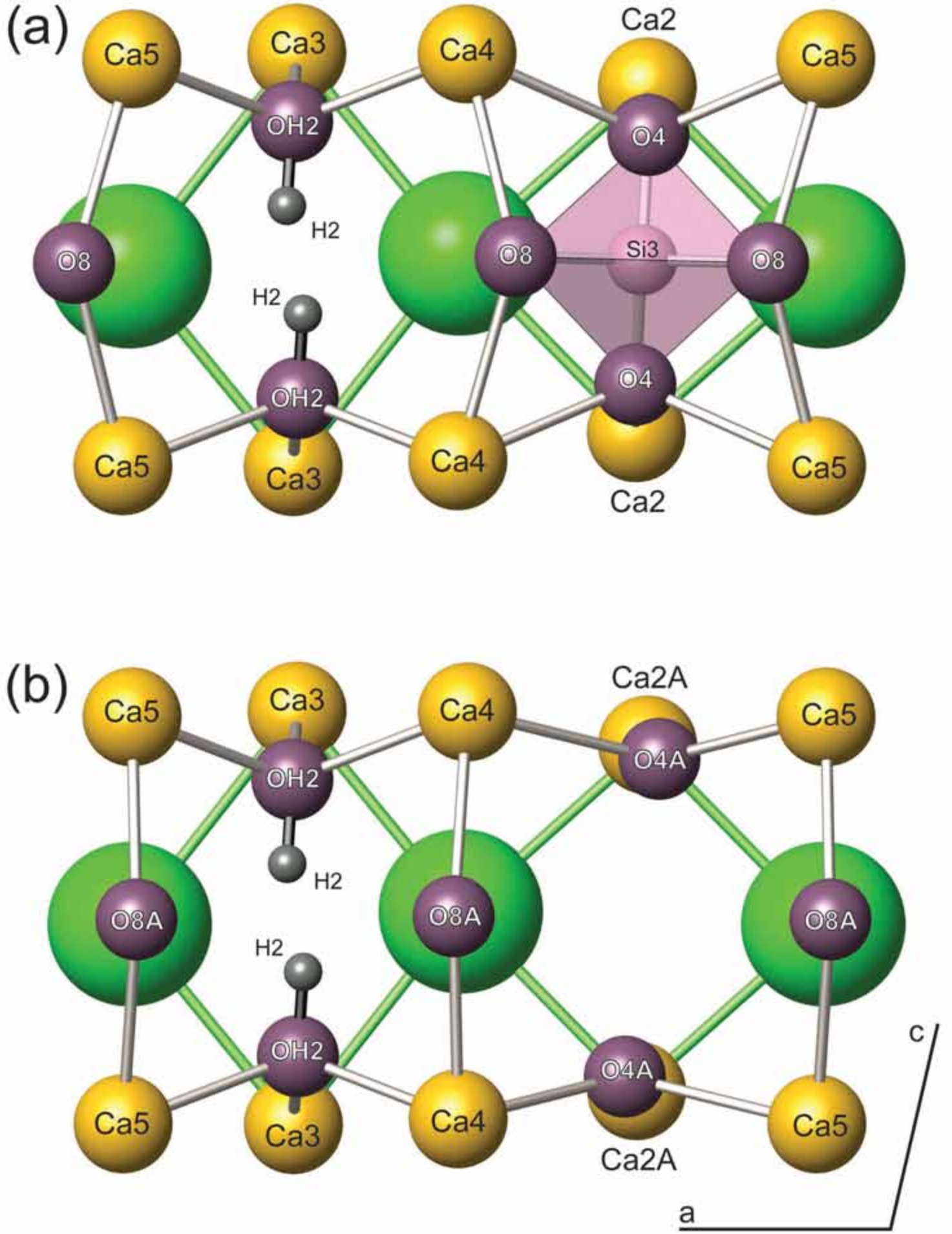
(a)
Ca5
Ca3
Ca4
Ca2
Ca5
OH2
O4
H2
O8
Si3
O8
H2
OH2
O4
Ca5
Ca3
Ca4
Ca5
Ca2
(b)
Ca5
Ca3
Ca4
Ca2A
Ca5
OH2
O4A
H2
O8A
O8A
O8A
H2
OH2
O4A
Ca5
Ca3
Ca4
Ca5
Ca2A
c
a